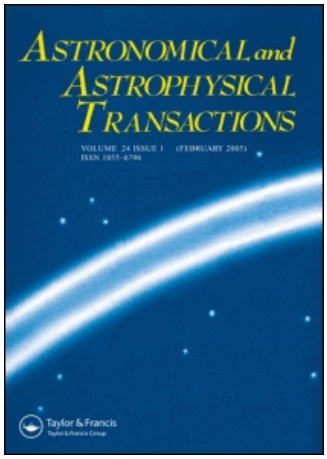

Astronomical & Astrophysical Transactions
The Journal of the Eurasian Astronomical Society
Publication details, including instructions for authors and subscription information:
http://www.informaworld.com/smpp/title~content=t713453505

Coronal Faraday rotation of occulted radio signals

M. K. Bird [a]
[a] Argelander-Institut für Astronomie, Universität Bonn, Bonn, Germany

Online Publication Date: 01 December 2007
To cite this Article: Bird, M. K. (2007) 'Coronal Faraday rotation of occulted radio signals', Astronomical & Astrophysical Transactions, 26:6, 441 - 453
To link to this article: DOI: 10.1080/10556790701595236
URL: http://dx.doi.org/10.1080/10556790701595236

Astronomical and Astrophysical Transactions
Vol. 26, No. 6, December 2007, 441–453

Coronal Faraday rotation of occulted radio signals

M. K. BIRD*

Argelander-Institut für Astronomie, Universität Bonn, Bonn, Germany

(Received 19 July 2007)

Faraday rotation (FR) observations of radio sources near solar conjunction yield information on the coronal magnetic field at heliospheric distances not reached by *in situ* exploration. Measurements of FR yield the rotation measure (RM), a wavelength independent quantity defined as the integral along the raypath of the product of the electron density times the raypath-parallel component of the magnetic field. Independent observations or models of the coronal electron density are required in order to extract information about the magnetic field. The radio sounding sources can be either artificial (spacecraft) or natural, but they must be at least partially linearly polarized. The most extensive campaign of coronal radio sounding polarization measurements using a spacecraft was the Helios Faraday Rotation Experiment, which was conducted over the duration of the Helios 1 (1974–1984) and Helios 2 (1976–1980) missions. Other coronal FR experiments have been carried out using natural continuum sources recently at the VLA and even as early as 1962 at the Pulkovo Radio Telescope. Pulsars were exploited to measure coronal RM at the MPIfR Effelsberg 100-m Telescope. Extending these single raypath observations, an ambitious project has been proposed to use the future LOFAR facility for constructing a coronal RM 'image'. Different time scales of FR variations are related to different physical phenomena. Among the observed effects are: (a) slow variations associated with the changing geometry and rotation of the corona; (b) random oscillations probably arising from a rich spectrum of coronal Alfvén waves; (c) rapid changes in RM caused by transient events such as coronal mass ejections (CMEs).

Keywords: Solar corona; Solar wind; Radio sounding; Faraday rotation

1. Introduction

Linear polarized electromagnetic waves propagating through a magnetized plasma undergo 'Faraday rotation' (FR) of their plane of polarization, which can be used to deduce the magnetic structure of the propagation medium. In particular, FR measurements of polarized radio signals passing near the Sun can be used to estimate the direction and strength of the magnetic field in the solar corona. Coronal FR has been measured over the rather narrow range of solar elongations defined by $2R_\odot \lesssim R \lesssim 15R_\odot$ ($R_\odot$ = solar radius), where R is the 'solar offset', the heliocentric distance of the solar proximate point along the radio ray path from the source to the observer on Earth. The lower bound is of instrumental nature, roughly defined by the onset of excessive solar sidelobe noise interference and rapidly changing FR. The outer bound is the distance at which the contribution from the solar corona typically exceeds that from the terrestrial ionosphere. Radio sounding FR measurements are thus the only proven means for

*Email: mbird@astro.uni-bonn.de

Astronomical and Astrophysical Transactions
ISSN 1055-6796 print/ISSN 1476-3540 online © 2007 Taylor & Francis
http://www.tandf.co.uk/journals
DOI: 10.1080/10556790701595236

studying the coronal magnetic field in the region of the solar wind transition to supersonic velocities.

2. Coronal Faraday rotation

The Faraday rotation *FR* (in the 'quasi-longitudinal' approximation) is defined as:

$$FR = \frac{K}{f^2} \int_S^{\oplus} N_e(s) B_s(s) ds \quad \text{radians} \tag{1}$$

where $K = 2.36 \times 10^4$ in both SI and cgs units, f is the radio frequency, B_s is the longitudinal component of the magnetic field along the ray path ($B_s = \vec{B} \cdot \hat{s}$), N_e is the electron density, and the integral in (1) is taken along the radio ray path from the source (S) to the ground station on Earth ($\oplus$).

The FR measurement technique can be described using the example of the Helios spacecraft, which underwent many solar conjunctions during the years 1974–1984. Measurements of coronal $FR = \Omega(t) - \Omega_0$ were obtained by tracking the *received* signal polarization angle q, referenced to the local horizon. Since the electric vector of the *transmitted* linearly polarized carrier signal from Helios was oriented perpendicular to the ecliptic, the polarization angle without the corona was thus defined to be $\Omega_0 = 0$. Transforming back to the ecliptic frame from the easily calculated angle p then yields $FR = \Omega(t) = p + q$, as shown schematically in figure 1. The FR measurement for natural radio sources is only slightly different. In this case the angle p is now the usual parallactic angle between local zenith and celestial north. One measures the interstellar value of the polarization angle Ω_0 when the source is at a large solar elongation and then obtains the coronal contribution as $FR = \Omega(t) - \Omega_0$ for the times t near superior conjunction.

The Faraday rotation *FR* is inversely proportional to the square of the radio frequency. For FR observations at any frequency, it is convenient to introduce another quantity, the Rotation Measure (RM):

$$FR = RM \cdot \lambda^2 \quad \text{radians} \tag{2}$$

where (in SI units):

$$RM = 2.63 \cdot 10^{-13} \int_s^{\oplus} N_e(s) B_s(s) ds \quad \text{rad m}^{-2} \tag{3}$$

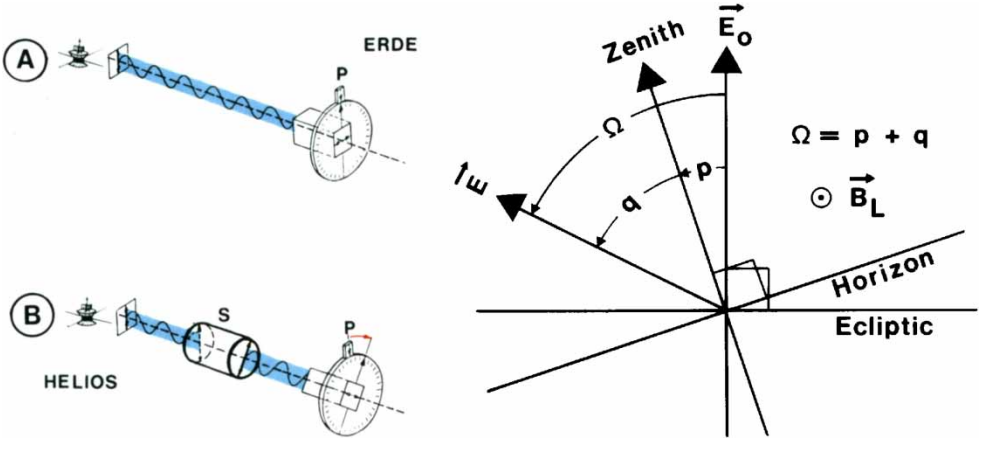

Figure 1. Helios Faraday rotation measurement. Left: Polarization angle measurement without (above) and with (below) the intervening solar corona; Right: reference in local and ecliptic systems, as viewed from an observer looking toward the spacecraft.

The values of FR produced from a medium with a rotation measure of $RM = 1$ rad m^{-2} are:

$$FR = 0.97^\circ \text{ at } 2.3\,\text{GHz } (\lambda = 0.13\,\text{m})$$
$$FR = 57.3^\circ \text{ at } 300\,\text{MHz } (\lambda = 1.0\,\text{m})$$
$$FR = 1432^\circ \text{ at } 60\,\text{MHz } (\lambda = 5.0\,\text{m})$$

Some properties of FR and RM include the following:

- FR is a signed quantity, either plus or minus depending on the orientation of the magnetic field along the ray path.
- The direction of rotation is called positive (counterclockwise) when the magnetic field points toward the observer, as sketched in figure 1, and negative (clockwise) when directed away from the observer.
- The value of coronal FR can become ambiguous, i.e. FR may in fact be $FR \pm n \times 180^\circ$, if the measurements cannot be made continuously.
- Contributions from N_e and B_s contribute equally to the integrated FR and RM and cannot be separated without independent measurements.
- Correction for the terrestrial ionosphere can become important if the solar offset $R \gtrsim 10 R_\odot$.

3. Radio sources for coronal Faraday rotation

3.1 *Extended continuum sources*

The most popular natural source for coronal FR experiments has been the Crab Nebula, the strongest source of linearly polarized emission in the sky, which approaches to within $5R_\odot$ during its superior conjunction in June of each year. The first attempt to measure coronal FR was made by Golnev *et al.* [1], who could set only an upper bound on the coronal contribution of $|FR| < 8^\circ$ (± 35 rad m^{-2} at $\lambda = 6.3$ cm). Later observations on the same source were reported by Sofue *et al.* [2], Berlin *et al.* [3], and Soboleva and Timofeeva [4].

Results of more recent dual-frequency coronal FR experiments using continuum sources at the Very Large Array (VLA) have been reported by Sakurai and Spangler [5, 6] and by Mancuso and Spangler [7, 8]. A more extensive campaign was conducted at the same facility in 2005 and the measurements compared with models of the coronal structure by Ingleby *et al.* [9]. An example from Spangler [10] using the source 3C228 is reproduced here in figure 2.

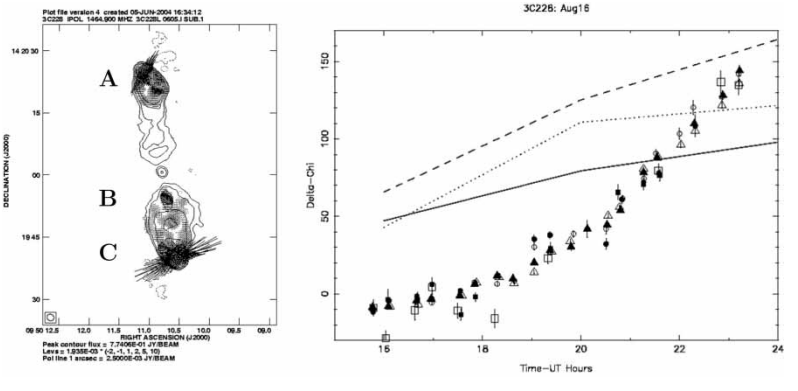

Figure 2. Coronal FR at the VLA. Left: Radio map of 3C228 showing the components A,B,C. Right: FR measurements on 16 August 2003 ($7.1R_\odot \rightarrow 6.2R_\odot$) of the components A (circles), B (squares) and C (triangles). Solid symbols are for 1465 MHz; open symbols for 1665 MHz (scaled to FR at 1465 MHz).

The temporal variation of all components (A,B,C) is the same, showing that changes in coronal RM over the projected separation distances of roughly 35,000 km are small. A relatively large increase in coronal rotation measure $\Delta FR \simeq 150^\circ \Rightarrow \Delta RM \simeq 62.5\ \mathrm{rad\,m^{-2}}$ was recorded on this particular day.

3.2 *Pulsars*

Strongly linearly polarized emission from pulsars has also been used for coronal FR measurements [11, 12]. Pulsars, although they are generally much weaker than the stronger continuum sources, have the remarkable attribute of turning themselves off for a large fraction of their pulse period so that the background emission can be conveniently calibrated. The background flux density at small solar elongation can exceed that of the source and is a sensitive function of the antenna orientation with respect to the Sun.

Figure 3 demonstrates the measurement technique, which is custom designed for each individual source, depending on the emission profile across the pulse window. The particular geometry and FR measurements for two pulsars located on either side of the Sun as shown in figure 4. The complex solar magnetic field, dominantly radial at these solar distances, but with sectors of both away and toward polarity, is responsible for the opposite polarities of coronal RM implied by figure 4.

3.3 *Spacecraft signals*

The spacecraft Pioneer 6 and 9 were the first to be used for successful measurements of coronal FR [13, 14]. By far the largest volume of spacecraft FR data was recorded within

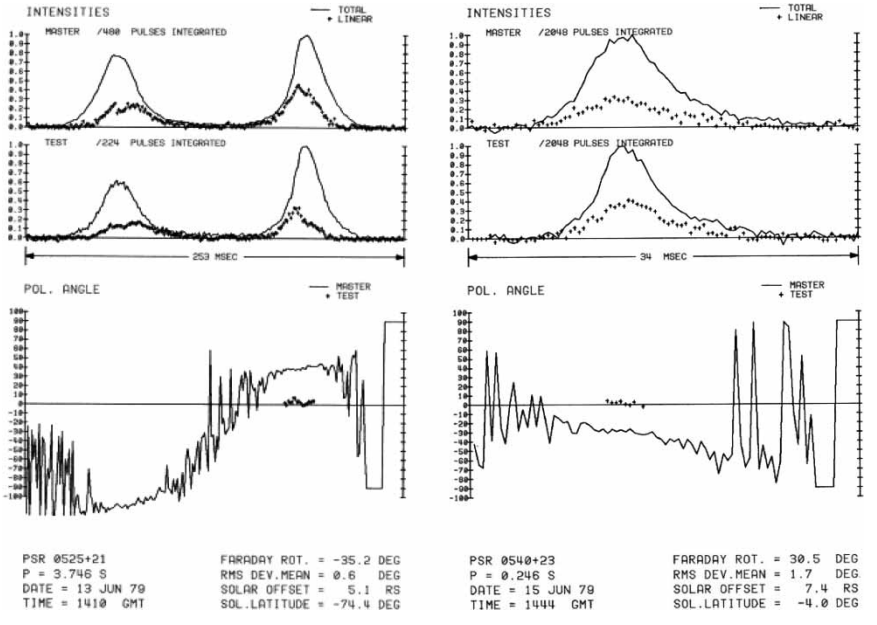

Figure 3. Pulsar pulse profiles. Left: PSR 0525+21; Right: PSR 0540+23. The duration of the pulse window is different for each pulsar. The upper curves show the total flux density and linearly polarized flux density for the 'master profile' (long integration, far from the Sun). The middle curves show the same quantities for the 'test profile' (short integrations near the Sun). The bottom curves show the polarization angle of the master (solid line) and the test (points, only when strong linear component available) profiles. The polarization angle difference (test–master) is the coronal Faraday rotation.

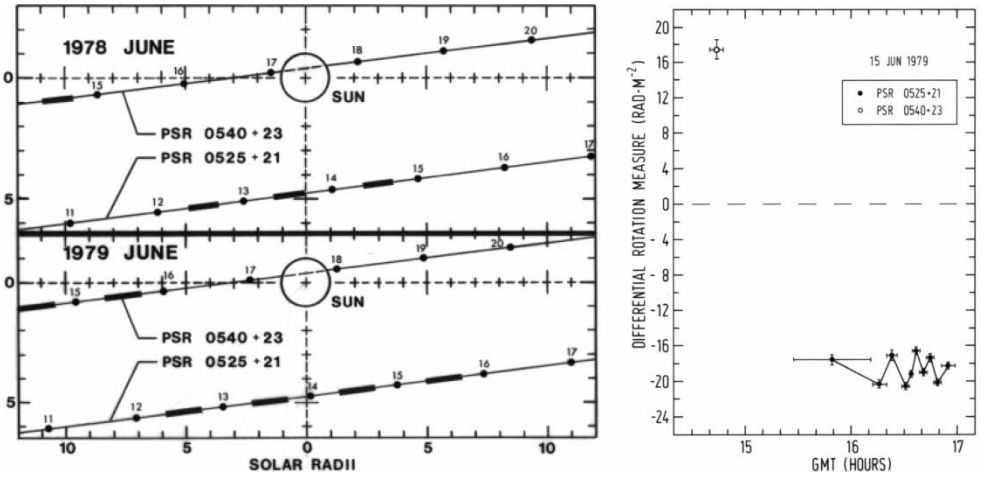

Figure 4. Coronal FR with pulsars, 1978-79. Left: Occultation geometry; Right: Measurements on 15 June 1979 when the coronal RM was positive on the east solar limb (PSR 0540) and negative on the west solar limb (PSR 0525).

the framework of the Helios Faraday Rotation experiment [15–17]. The unexpectedly long lifetime of the Helios probes enabled studies to extend from deepest solar activity minimum into the following maximum and beyond. Helios FR data have now been made available in an online archive.

Only the large Goldstone station of the NASA Deep Space Network (DSN) and the 100 m Effelsberg Radio Telescope of the Max-Planck-Institut für Radioastronomie (MPIfR) were used during the first two Helios mission years. Starting in 1977, after the DSN added automatic tracking polarimeters at the large stations in Canberra and Madrid, some of the coronal FR experiments could be conducted on a continuous (global) basis.

Figure 5 shows an ecliptic plane view of the Helios orbits in a Sun/Earth fixed system. Since the Helios spacecraft were in the ecliptic plane, all solar occultations proceeded diametrically along a solar radial, either of short duration from west to east limb near perihelion, or a more lengthy occultation phase in the reverse direction near aphelion. The short-period, zero-inclination, heliocentric orbits of the two identical Helios spacecraft were ideal for conducting

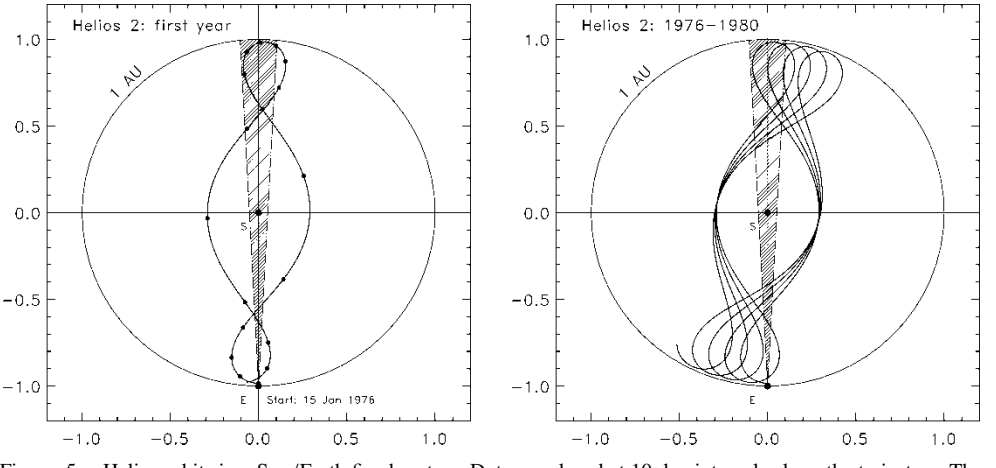

Figure 5. Helios orbits in a Sun/Earth fixed system. Dots are placed at 10 day intervals along the trajectory. The shaded region of space bounded by a solar elongation ±3° is roughly the region where coronal FR was recorded. Left: Helios 1 during its first year; Right: Helios 2 during its operational lifetime 1976–1980.

coronal radio science investigations during the recurring solar occultations. Helios 1, with an original design lifetime of 18 months, was launched 10 December 1974 and underwent a total of 10 solar conjunctions before it failed in 1985. Helios 2 was tracked regularly from its launch on 15 January 1976 until it ceased operating on 3 March 1980. The perihelion for Helios 2 was 0.29 AU, compared to the 0.31 AU of Helios 1.

The following section provides a brief overview of the Helios coronal FR measurements on various time scales and their implications for the spatial structure and temporal variability of the coronal plasma and magnetic field.

4. FR variations over different time scales

The time scales of FR variations, observed during virtually all occultations, provide information on various physical phenomena in the solar corona:

4.1 *Slowly-varying background*

The gradual rise and fall in FR results from the superposition of effects from the changing ray path offset and the rotation of the quasi-static corona. Figure 6 shows such slow FR variations observed during the Helios 1 solar conjunction in December 1981. Complete global coverage without data gaps between ground stations was achieved during the the 1981 solar conjunction. Slight differences in the FR measured at two ground stations, seen during the overlap intervals, may be attributed to the different ionospheric contributions at each individual ground station.

Pätzold *et al.* [18] utilized FR measurements from 1975–76 for a determination of the mean coronal magnetic field during solar minimum. Figure 7 shows the model for their analysis,

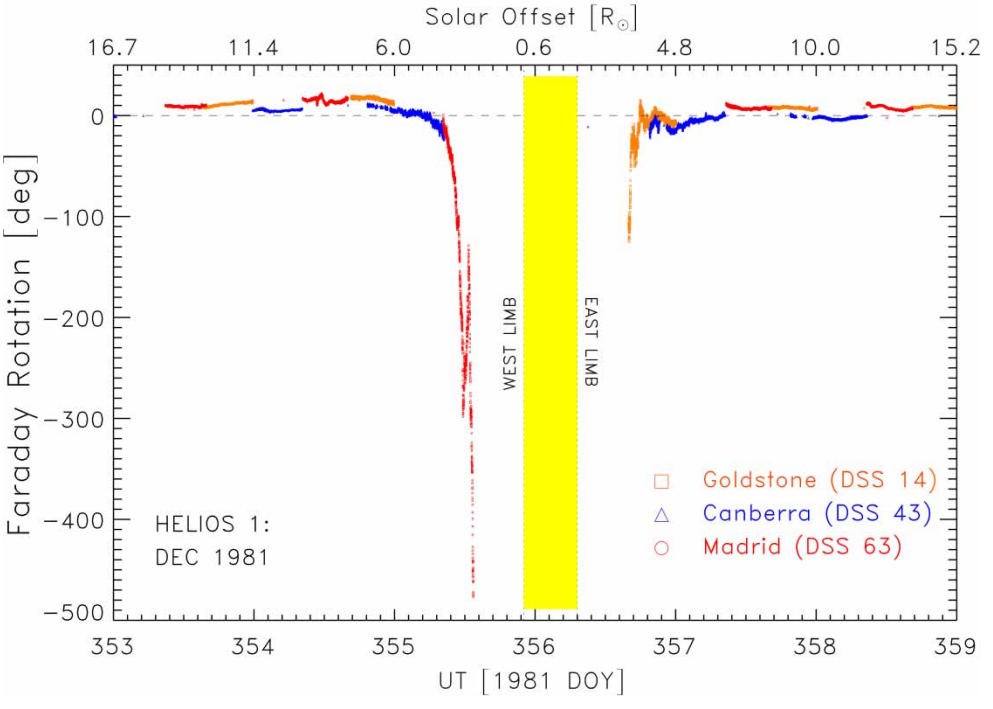

Figure 6. Coronal FR observed with Helios 1 during the solar occultation in December 1981. Observations conducted at each 70-m ground station of the NASA Deep Space Network (DSN) are marked with different symbols.

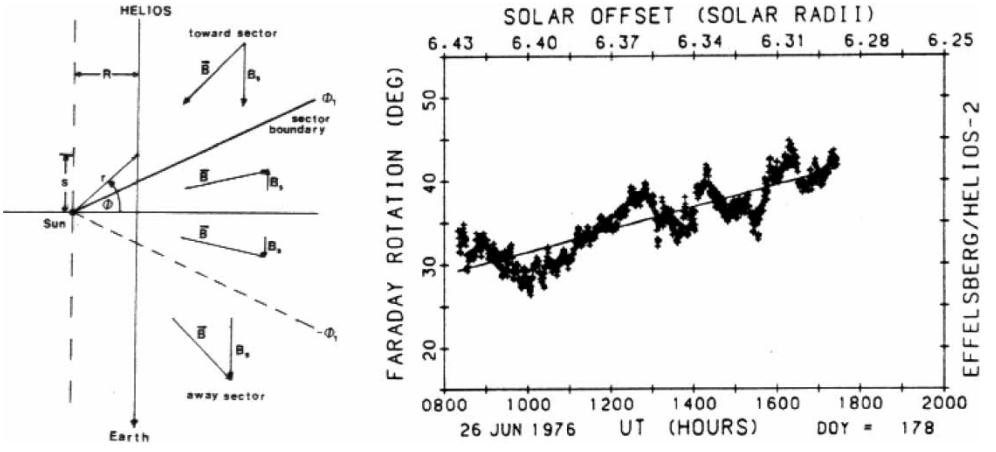

Figure 7. Helios FR measurements. Left: Coronal magnetic field model used for analysis; Right: Typical tracking pass for $R \simeq 6.4 R_\odot$ ($\langle FR \rangle = 35.4°$, $\sigma_{FR} = 2.1°$).

together with an example of a typical tracking pass at the MPIfR 100-m Radio Telescope in 1976. The radial magnetic field of the solar corona is assumed to have sectors of either toward or away polarity. Figure 7 shows an example where only one sector boundary on the solar limb is intersected by the radio ray path from Helios to Earth. The ray path integration close to the proximate point, with equal length segments of positive and negative magnetic field along the ray path, will yield net zero FR because of symmetry. Maximum FR (negative or positive, depending on the polarity) will be measured when the sector boundary is exactly at the limb. This particular constellation for $|FR_{max}|$ will be achieved only by coincidence during a single given occultation. However, if one plots data from many occultations, a maximum FR envelope will begin to make itself apparent.

Figure 8 shows the data $|FR(R)|$ and the magnetic field model derived from the data. The slope of the maximum envelope in figure 8 (left panel) was found to be -4.15. Combining this with an assumption about the spherical distribution of coronal electron density, one is able to derive the radial dependence of the coronal magnetic field. If both B_r and N_e can be taken as

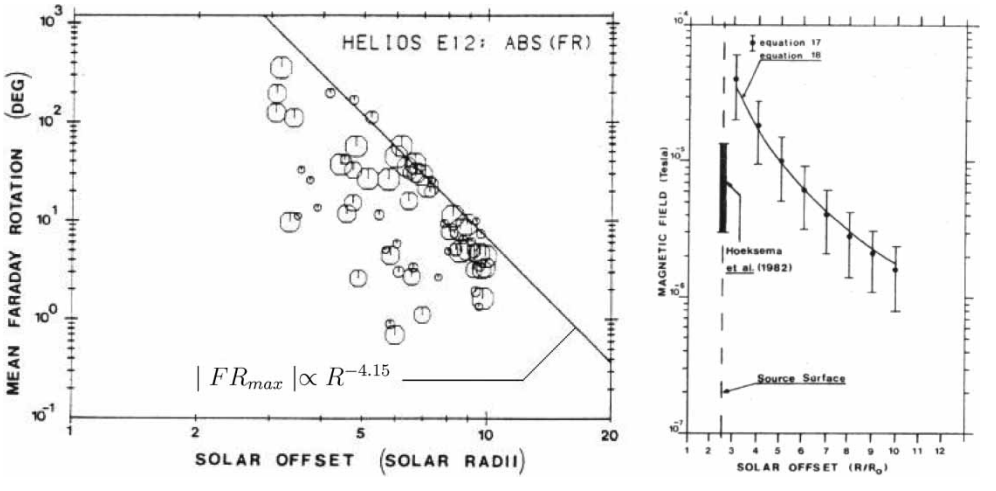

Figure 8. Mean coronal magnetic field strength at solar minimum. Left: Measurements of $|FR|$ with maximum envelope; Right: Derived radial dependence of the coronal magnetic field.

simple power laws:

$$B_r = B_0 \left[\frac{R_\odot}{r}\right]^{\beta_1}; \quad N_e = N_0 \left[\frac{R_\odot}{r}\right]^{\beta_2} \tag{4}$$

then it is found that:

$$|FR_{max}| = |FR_0| \left[\frac{R_\odot}{r}\right]^{\beta_1+\beta_2-1} \tag{5}$$

so that $\beta_1 \simeq 2.65$ when the electron density exponent $\beta_2 \simeq 2.5$. The empirical formula shown in figure 8 (right panel) was actually obtained from a fit to a two-term expression

$$B_r = 6 \left[\frac{R_\odot}{r}\right]^3 + 1.8 \left[\frac{R_\odot}{r}\right]^2 \text{gauss} \tag{6}$$

which implies that the coronal magnetic field in the range from 3–10 $R_\odot$ is essentially a hybrid between the strongest multipole of the Sun's internal field (dipole – falloff exponent 3) and the interplanetary magnetic field (pure radial – falloff exponent 2).

4.2 *Random oscillations*

Fluctuations are seen in all of the Helios FR data and tend to decrease with distance from the Sun. The primary causal agent is suspected to be coronal Alfvén waves [19–29].

The fluctuations are conveniently quantified in terms of FR spectra, with a given amplitude and spectral index (i.e. the falloff exponent with fluctuation frequency). Figure 9 shows a series of FR temporal spectra at various solar offset distances.

The FR power spectra are usually simple power laws over the observed range of temporal frequencies from 1 to 200 mHz. The integral over the spectra of figure 9 (left panel), a measure of the FR fluctuation variance, decreases with solar distance. Hollweg *et al.* [19] concluded that more than 90% of the FR variance can be attributed to fluctuations of the magnetic field rather than the electron density. The spectral index (figure 9, right panel) also displays a decrease

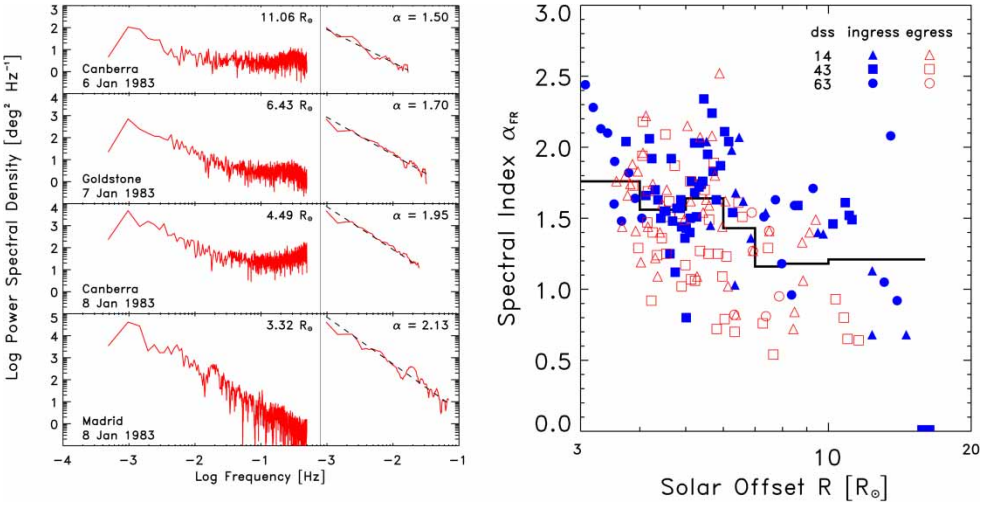

Figure 9. Faraday rotation fluctuations. Left: FR power spectra at four different solar offset distances with indicated fits to smoothed spectra for the spectral index over the interval from 1 to 50 mHz; Right: FR spectral index as a function of solar offset.

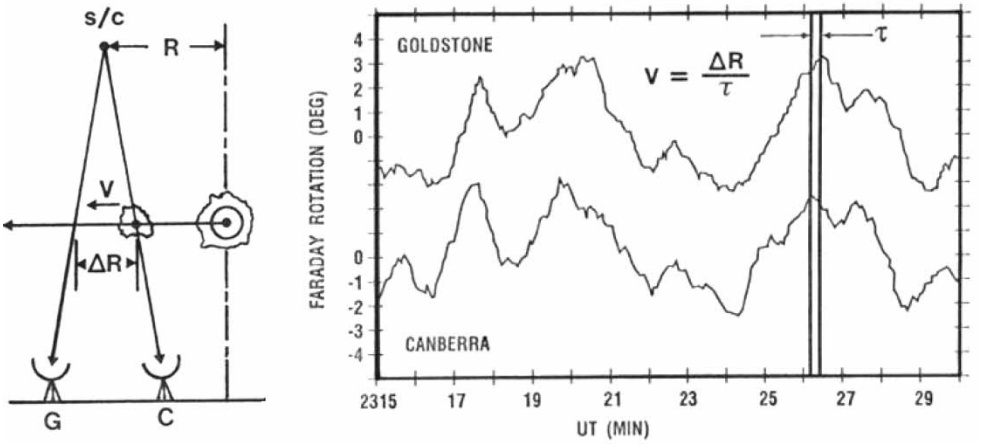

Figure 10. Estimation of characteristic coronal velocity from two-station correlation analysis. Left: Sketch showing observation geometry; Right: Measurements recorded simultaneously at the DSN Goldstone and Canberra ground stations. Knowing the coronal separation (ΔR) of the two ray paths, the observed time delay ($\tau \simeq 10$ s) can be used to derive a characteristic radial velocity V.

(flatter spectra) with solar distance. Both of these trends were found to be largely independent of the level of solar activity.

The FR fluctuations can be used to determine characteristic coronal velocities if simultaneous observations are available from widely-separated ground stations. Figure 10 shows a typical example where the fluctuations at Goldstone replicate the same signature at Canberra, but with a certain time lag τ.

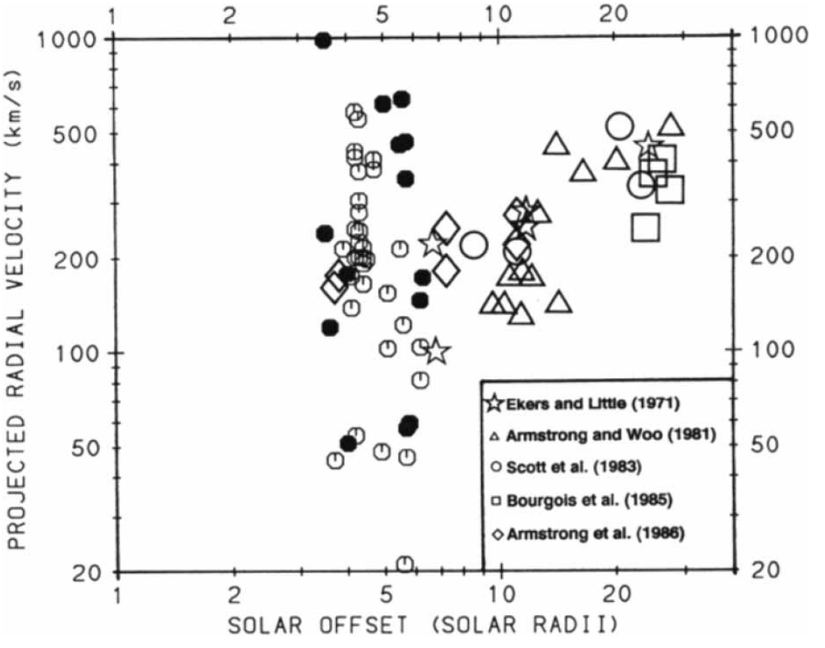

Figure 11. Coronal velocities derived from correlation time lag observations at widely-separated ground stations. The velocities reported from the studies denoted in the inset are all positive outward and tend to lie close to the profile expected for the solar wind velocity. The FR data are displayed as circles that generally lie higher the other estimates and are either open (radially outward directed velocity) or solid (radially inward directed velocity).

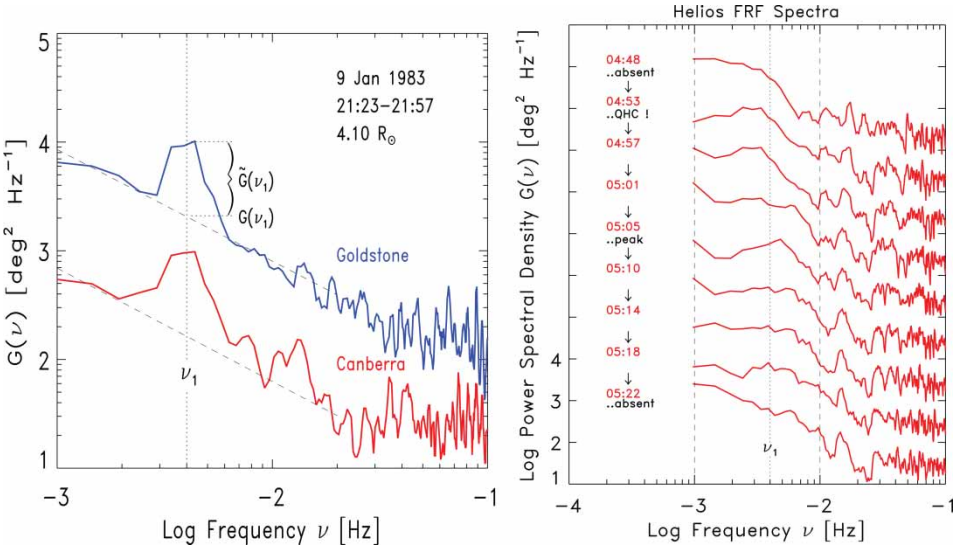

Figure 12. Faraday rotation power spectra with a quasi-harmonic component. Left: Power spectra with obvious peak near 4 mHz (period: 4.2 minutes), recorded simultaneously at the DSN Goldstone and Canberra ground stations during an interval of station overlap; Right: A time series of FR fluctuation spectra showing the build-up and decay of the quasi-harmonic component.

The radial velocities inferred from all available FR data are compared with velocities derived from other radio sounding data in figure 11.

A study by Bird *et al.* [30] reported that 30% of the velocities determined from two-station cross correlations were directed *radially inward toward the Sun*. It was concluded that the characteristic velocities derived from the FR fluctuations are associated with the Alfvén velocity V_a rather than the solar wind velocity V_{sw}. In the region applicable to these observations, where $|V_a| \gg |V_{sw}|$, it is entirely possible that negative velocities could be occasionally detected.

Another serendipitous discovery from the Helios FR data set is shown in figure 12. Whereas the FR temporal spectra are generally power laws, a distinct maximum in the spectrum is sometimes observed at temporal frequencies near $\nu_1 \simeq 4$mHz (periodicies near 4–5 minutes) that has been called the 'quasi-harmonic component' or QHC [23, 31]. Although the sporadic QHC is ephemeral (e.g. figure 12, right panel), seldom lasting longer than 30 minutes, the QHC frequency remains essentially the same regardless of solar distance. The amplitude of the QHC line can be 3–4 times stronger than the background FR spectrum at the same frequency and falls off with R at the same rate as the background. The constant value of the frequency ν_1 and the radial falloff with the background imply that the QHC are caused by isolated Alfvén wave trains that occasionally occupy a significant segment of the radio ray path.

4.3 *FR discontinuities*

Occasional abrupt jumps are observed in the FR observations. These signatures are assumed to be caused by transient events such as coronal mass ejections (CMEs). In fact, such 'FR transients' were observed [13] even before their optical manifestations were widely recognised from the orbiting coronagraph observations on Skylab. Five distinct FR events observed during the 1979 Helios solar conjunctions were associated with the passage of white-light CMEs through the signal ray path [32]. One example from this study is presented in figure 13. Bird

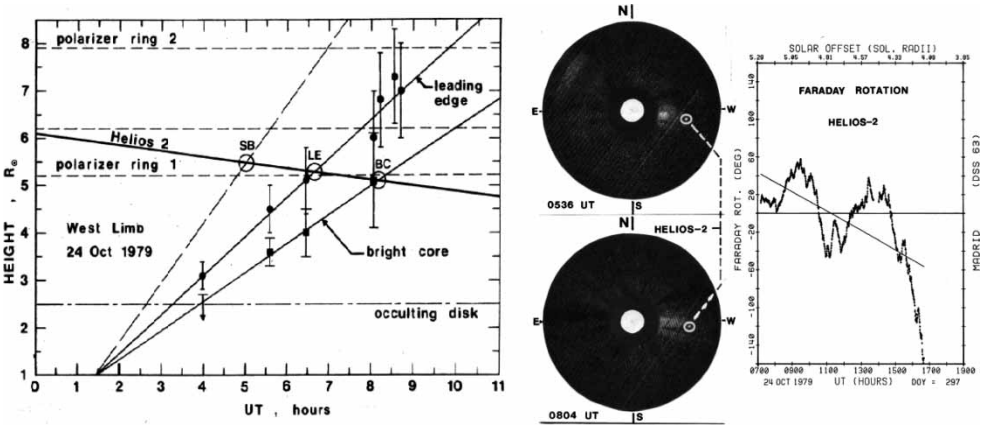

Figure 13. Simultaneous white-light and FR observations of a CME on 24 October 1979. Left: Time-height diagram showing the solar distance of the Helios 2 ray path and the radial position of the CME leading edge and bright core; Right: White-light images from the Solwind coronagraph compared with FR measurements recorded during the CME passage through the Helios/Earth line-of-sight.

et al. [32] concluded that a one-to-one correspondence existed between the white-light CMEs and the FR transients observed with Helios and earlier with Pioneer 9. Although it has been speculated that the FR transients can be associated with interplanetary sector boundaries [33], numerical calculations by Pätzold and Bird [34] have shown that the time scales corresponding to sector boundary passage are much too slow to reproduce the abrupt large deviations observed in the FR records.

5. Coronal FR mapping – outlook

A significant disadvantage of the FR observational technique described in the preceding sections is its restriction to only a single line of sight. If an abundance of polarized sources were available and if the ground-based observing network were capable of observing these sources in a near simultaneous mode, one could conceivably even generate a 'Faraday rotation map' of the corona. How such an FR map might look is shown in figure 14.

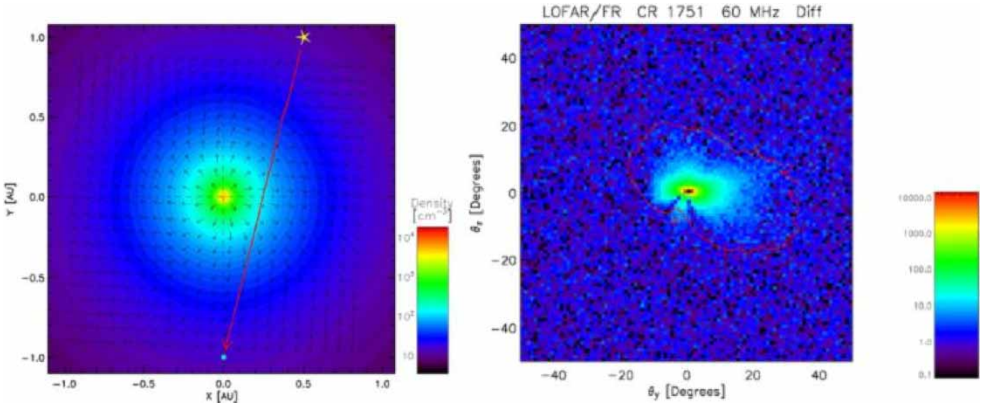

Figure 14. Faraday rotation map of the solar corona. Left: Sketch of the geometry showing the radio ray path from a given source through a modelled region of the solar corona to the observer on earth; Right: FR map (60 MHz) on the plane of the sky [Courtesy of J. Kasper, private communication].

Figure 14 shows a simulation of the expected FR observed on Earth at $f = 60$ MHz from many radio rays passing through a specified coronal distribution of electron density and magnetic field. Only the magnitude of the Faraday rotation ($|FR|$) is plotted. The contours of constant FR in figure 14 extend out to solar elongations of 30° and beyond. Of course, measurements of coronal FR at these distances require precise corrections for ionospheric FR, which can reach thousands of degrees at a radio frequency of 60 MHz. Ongoing feasibility studies performed in association with future low frequency arrays (LOFAR, MWA) address the possibility of using such multi-source FR observations to predict the magnetic polarity (and thus the geoeffectivity) of CMEs directed at Earth.

6. Summary

The time scales of FR variations provide information on various physical phenomena: (a) slowly-varying rise and fall associated with the changing ray path offset, combined with the rotation of the quasi-static corona; (b) ubiquitous random oscillations with higher fluctuation amplitude at smaller solar offset distances, probably caused by coronal Alfvén waves; (c) occasional nearly discontinuous jumps in the polarization angle, most likely caused by transient events such as coronal mass ejections (CMEs).

Coronal Faraday rotation observations have provided valuable clues about the quiet and disturbed magnetic structure of the solar corona in the critical radial range $2R_{\odot} < R < 15R_{\odot}$. Among these important new results are an empirical model for the background coronal magnetic field and the convincing evidence for coronal Alfvén waves.

An extension of these observations to FR sky maps, which would greatly enhance the diagnostic capability of the FR measurements, is being investigated. The technical constraints associated with this effort are formidable but not prohibitive. It will be interesting to monitor the continuing developments in this area of research over the next few years.

Acknowledgements

This paper presents results of research partly funded by the Deutsche Forschungsgemeinschaft (DFG) under a cooperative program between the DFG and the Russian Foundation of Basic Research (RFBR). Valuable contributions to the Helios FR Experiment from the Helios Project Team, the German Space Operations Centre (GSOC) of the Deutsches Zentrum für Luft- und Raumfahrt (DLR), the Max-Planck-Institute für Radioastronomie (MPIfR), the NASA Deep Space Network (DSN), and the Multi-Mission Radio Science Support Team at the Jet Propulsion Laboratory (JPL) are acknowledged.

References

[1] V.Y. Golnev, Y.N. Pariiskii and N.S. Soboleva, Izv. Glavnoi Astron. Obs. Pulkove **23** 22 (1964).
[2] Y. Sofue, K. Kawabata, F. Takahashi and N. Kawajiri, Solar Phys. **50** 465 (1976).
[3] A.B. Berlin, D.V. Korolkov, Y.N. Pariiskii, N.S. Soboleva and G.M. Timofeeva, Pisma Astron. Zh. **4** 191 (1978); [Sov. Astron. Lett. **4**(2) 102 (1978)].
[4] N.S. Soboleva and G.M. Timofeeva, Pisma Astron. Zh. **9** 409 (1983); [Sov. Astron. Lett. **9**(4) 216 (1983)].
[5] T. Sakurai and S.R. Spangler, Radio Sci. **29** 635 (1994).
[6] T. Sakurai and S.R. Spangler, Astrophys J. **434** 773 (1994).
[7] S. Mancuso and S.R. Spangler, Astrophys J. **525** 195 (1999).
[8] S. Mancuso and S.R. Spangler, Astrophys J. **539** 480 (2000).
[9] L.D. Ingleby, S.R. Spangler and C.A. Whiting, Astrophys J. in press (2007).
[10] S.R. Spangler, Space Sci. Rev. **121** 189 (2005).
[11] M.K. Bird, E. Schrüfer, H. Volland and W. Sieber, Nature **283** 459 (1980).
[12] M.K. Bird, in *Solar Wind Four* [MPAE-W-100-81-31], H. Rosenbauer (ed.), 78 (1981).

[13] G.S. Levy, T. Sato, B.L. Seidel, C.T. Stelzried, J.E. Ohlson and W.V.T. Rusch, Science **166** 596 (1969).
[14] C.T. Stelzried, G.S. Levy, T. Sato, W.V.T. Rusch, J.E. Ohlson, K.H. Schatten and J.M. Wilcox, Solar Phys. **14** 440 (1970).
[15] H. Volland, M.K. Bird, G.S. Levy, C.T. Stelzried and B.L. Seidel, J. Geophys. **42** 659 (1977).
[16] G.S. Levy, H. Volland, M.K. Bird, C.T. Stelzried and B.L. Seidel, in *The HELIOS Solar Probes: Science Summaries* [NASA-TM 82005], J.H. Trainor (ed.), 85 (1980).
[17] M.K. Bird and P. Edenhofer, in *Physics of the Inner Heliosphere*, R. Schwenn, E. Marsch (eds), Springer-Verlag, Berlin, 13 (1990).
[18] M. Pätzold, M.K. Bird, H. Volland, G.S. Levy, B.L. Seidel and C.T. Stelzried, Solar Phys. **109** 91 (1987).
[19] J.V. Hollweg, M.K. Bird, H. Volland, P. Edenhofer, C.T. Stelzried and B.L. Seidel, J. Geophys. Res. **87** 1 (1982).
[20] A.I. Efimov, I.V. Chashei, V.I. Shishov and M.K. Bird, Pisma Astronom. Zh. **19** 143 (1993); [Astron. Lett. **19** 57 (1993)].
[21] A.I. Efimov, M.K. Bird, V.E. Andreev and L.N. Samoznaev, Pisma Astronom. Zh. **22** 874 (1996); [Astron. Lett. **22** 785 (1996)].
[22] A.I. Efimov, V.E. Andreev, L.N. Samoznaev, I.V. Chashei and M.K. Bird, Astronom. Zh. **76** 312 (1999); [Astron. Rep. **43** 267 (1999)].
[23] A.I. Efimov, L.N. Samoznaev, V.E. Andreev, I.V. Chashei and M.K. Bird, Pisma Astronom. Zh. **26** 630 (2000); [Astron. Lett. **26** 544 (2000)].
[24] V.E. Andreev, A.I. Efimov, L.N. Samoznaev and M.K. Bird, in *Solar Wind Eight [AIP Conf. Proc. 382]*, D. Winterhalter *et al*. (eds), AIP Press, Woodbury, NY/USA, 34 (1996).
[25] V.E. Andreev, A.I. Efimov, L.N. Samoznaev, I.V. Chashei and M.K. Bird, Adv. Space Res. **20**(1) 65 (1997).
[26] V.E. Andreev, M.K. Bird, A.I. Efimov, L.N. Samoznaev and I.V. Chashei, Pisma Astronom. Zh. **23** 222 (1997); [Astron. Lett. **23** 194 (1997)].
[27] V.E. Andreev, M.K. Bird, A.I. Efimov, I.V. Chashei and L.N. Samoznaev, Astronom. Zh. **74** 263 (1997); [Astron. Rep. **41** 227 (1997)].
[28] V.E. Andreev, A.I. Efimov, L.N. Samoznaev, I.V. Chashei and M.K. Bird, Solar Phys. **176** 387 (1997).
[29] L.N. Samoznaev, A.I. Efimov, V.E. Andreev, I.V. Chashei and M.K. Bird, in *Proceedings of the International Symposium Space Plasma Studies by In-situ and Remote Measurements [Physics and Chemistry of the Earth, Part C, 25]*, M.I. Verigin (ed.), Springer-Verlag, Heidelberg, 107 (2000).
[30] M.K. Bird, H. Volland, A.I. Efimov, G.S. Levy, B.L. Seidel and C.T. Stelzried, in *Solar Wind Seven*, E. Marsch, R. Schwenn (eds), Pergamon Press, Oxford, 147 (1992).
[31] I.V. Chashei, M.K. Bird, A.I. Efimov, V.E. Andreev and L.N. Samoznaev, Solar Phys. **189** 399 (1999).
[32] M.K. Bird, H. Volland, R.A. Howard, M.J. Koomen, D.J. Michels, N.R. Sheeley, Jr., J.W. Armstrong, B.L. Seidel, C.T. Stelzried and R. Woo, Solar Phys. **98** 341 (1985).
[33] R. Woo, Geophys. Res. Lett. **24** 97 (1997).
[34] M. Pätzold and M.K. Bird, Geophys. Res. Lett. **25** 2105 (1998).